INTERSCALE ENERGY TRANSFER IN TURBULENT STRIPE STRUCTURE IN A TRANSITIONAL PLANE COUETTE FLOW

Yuki Yamaguchi
Department of Mechanical Engineering
Shibaura Institute of Technology
Toyosu 3-7-5, Tokyo, 135-8548 Japan
email: aa21100@shibaura-it.ac.jp

Takahiro Tsukahara
Department of Mechanical and Aerospace Engineering, Tokyo University of Science
Yamazaki 2641, Chiba, 278-8510 Japan
email: tsuka@rs.tus.ac.jp

Takuya Kawata
Department of Advanced Mechanical Engineering
Shibaura Institute of Technology
Toyosu 3-7-5, Tokyo, 135-8548 Japan
email: kawata@shibaura-it.ac.jp

ABSTRACT

Transitional plane wall-bounded shear flows exhibit intermittent turbulent structures in which oblique band-like turbulent regions and quasi-laminar regions form a regular alternating pattern, often referred to as the turbulent stripe structure. The quasi-laminar regions are accompanied by secondary flows along the band-like turbulent regions, the spatial scales of which are more than one order of magnitude larger than those of the turbulent structures. In the present study, we perform a direct numerical simulation of a transitional plane Couette flow and investigate the interscale energy transfers between the smaller-scale turbulence and the larger-scale secondary flows to elucidate the role of the nonlinear interactions between these two distinct scales in sustaining the turbulent stripe structure. We show that the turbulent energy is transferred from the smaller- to larger-scales in the band-like turbulent regions, suggesting that the large-scale secondary flows in the quasi-laminar gaps are produced from the smaller-scale turbulence localised in the band-like region.

INTRODUCTION

Planar wall-bounded shear flows, such as plane Poiseuille and Couette flows, at transitional Reynolds numbers exhibit characteristic flow patterns with alternating turbulent and (quasi-)laminar regions, where the turbulent phase is the oblique band-like regions with streaks and vortices and the gaps between them are paved by the quasi-laminar regions (see, for example, Tuckerman *et al.*, 2020, and the references therein). The regular laminar–turbulent alternations typically have spatial scales on the order of several tens of the channel height, which is more than an order of magnitude larger than the typical scales of streaks and vortices within the turbulent bands. Furthermore, the quasi-laminar phase is accompanied by secondary flows along the laminar–turbulent interface (e.g., Barkley & Tuckerman, 2007; Duguet & Schlatter, 2013; Couliou & Monchaux, 2015; Klotz *et al.*, 2021), which clearly indicates a break of symmetry in the spanwise direction as the turbulent bands are oblique to the streamwise direction.

The role of interaction between the large-scale secondary flows in the quasi-laminar phase and small-scale structures in the turbulent bands is a crucial factor in elucidating the origin and sustaining mechanism of this laminar–turbulent coexisting state. Duguet & Schlatter (2013) attributed the growth of a turbulent spot into an oblique turbulent band to advections by secondary flows in the oblique direction. Xiao & Song (2020) suggested that an inflectional instability of the oblique mean flow around the 'head' of a turbulent band is responsible for its growth in an oblique direction. These studies suggest that the large-scale secondary flows are necessary for triggering and sustaining the localised turbulence. The investigation by Parente *et al.* (2022) on optimal disturbance growths showed, on the other hand, that the large-scale flows emerge from initial states with spatially-localised perturbations and eventually lead to efficient generations of turbulent bands, suggesting that localised turbulence gives rise to the large-scale flows, in contrast to the aforementioned studies. Furthermore, some earlier studies focusing on turbulent energy transfers in turbulent stripe structures reported the energy transfers from smaller to larger scales (Fukudome *et al.*, 2009; Nimura *et al.*, 2019; Gomé *et al.*, 2023), although the physical process that such energy transfers represent is still not clear. Thus, the role of nonlinear coupling between the large-scale secondary flows and small-scale localised turbulence in the generation and sustaining of the turbulent bands still remains not fully elucidated.

In this study, we investigate interscale energy transfers between the large-scale secondary flows and localised turbulent structures based on a DNS dataset of a transitional plane Couette flow, aiming to elucidate the role of interactions between the large-scale flows and localised turbulence in sustaining turbulent band. The analysis is based on the framework proposed by Kawata & Alfredsson (2018, 2019), where velocity fluctuations are decomposed into large- and small-scale part and energy transfers due to their interactions are formulated.

NUMERICAL SETUP FOR DNS

In the configuration of the present DNS, the plane Couette flow is driven by two parallel flat plates separated by distance h, as shown in Fig. 1; the bottom wall is stationary and the

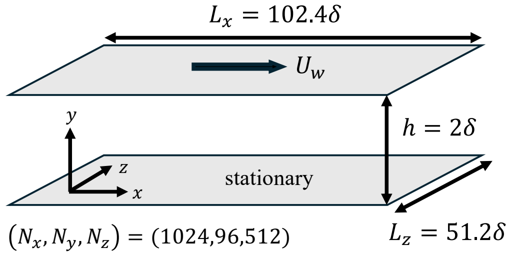

Figure 1. Configuration of plane Couette flow.

top wall is translating with a constant speed U_w. The coordinate origin is placed on the stationary bottom wall and we denote the streamwise, wall-normal, and spanwise directions as x-, y, and z-directions, respectively. The governing equations are the continuity equation and the Navier-Stokes equation for incompressible fluid non-dimensionalised based on the wall-translating speed U_w and the full channel gap h:

$$\frac{\partial U_i^*}{\partial x_i^*} = 0 \tag{1a}$$

$$\frac{\partial U_i^*}{\partial t^*} + U_m^* \frac{\partial U_i^*}{\partial x_m^*} = -\frac{\partial P^*}{\partial x_i^*} + \frac{1}{Re_\mathrm{w}} \frac{\partial^2 U_i^*}{\partial x_m^{*2}}, \tag{1b}$$

where the superscript $*$ indicates non-dimensionalised quantities, U_i is instantaneous velocity in the x_i-direction (when not using the index notation, we denote the velocity components in the x-, y- and z-directions as U, V and W, respectively), P is instantaneous pressure, and Re_w is the Reynolds number defined based on U_w and h: $Re_\mathrm{w} = U_\mathrm{w} h/\nu$ (ν is the kinematic viscosity of the fluid).

The domain sizes in the x- and z-directions are $(L_x, L_z) = (51.2h, 25.6h)$ and the number of the grid points in each direction is $(N_x, N_y, N_z) = (1024, 96, 512)$. Non-slip and periodic conditions are applied on the walls and the other boundaries, respectively. The numerical setup of the present DNS is basically the same as in our earlier computations (see, for example, Tsukahara *et al.*, 2005). The computation was initiated with an instantaneous velocity field of fully-developed plane Couette turbulence at $Re_\mathrm{w} = 8600$, and the intermittent turbulence with a turbulent stripe was obtained by gradually decreasing Re_w to the target Reynolds number $Re_\mathrm{w} = 1500$.

ENERGY TRANSFER ANALYSIS

In the present analysis, we investigate the energy transfer between the large-scale secondary flow and the smaller-scale localised turbulence based on the framework proposed by Kawata & Alfredsson (2018, 2019). First, we introduce the Reynolds decomposition: $U_i = \overline{U_i} + u_i$, where $\overline{U_i}$ is the mean velocity averaged in the x- and z-directions and in time and u_i is the fluctuation. In order to investigate the energy transfer between the large-scale secondary flows and small-scale turbulence, we further decompose the velocity fluctuation u_i into its large- and small-scale part u_i^L and u_i^S by a spatial filtering with the cutoff wavenumber at $k_z = 2\pi/L_z$:

$$u_i^L = \frac{2\pi}{L_z} \sum_{|n|\le 1}^{n} \widetilde{u}_{i,n} e^{-jk_{z,n}z}, \quad u_i^S = \frac{2\pi}{L_z} \sum_{|n|\ge 2}^{n} \widetilde{u}_{i,n} e^{-jk_{z,n}z} \tag{2}$$

where n is an integer, j is the imaginary unit, and $\widetilde{u}_{i,n}$ is the spanwise Fourier coefficient of u_i at the n-th wavenumber $k_{z,n} = 2\pi n/L_z$. As u_i^L and u_i^S do not share any common wavenumber, the cross correlations between them are zero for any combination of velocity components: $\overline{u_i^L u_j^S} = \overline{u_i^S u_j^L} = 0$. Hence, the Reynolds stresses $\overline{u_i u_j}$ are decomposed into their large- and small-scale parts as $\overline{u_i u_j} = \overline{u_i^L u_j^L} + \overline{u_i^S u_j^S}$. As will be demonstrated by Fig. 2, the cutoff wavenumber $k_{z,1} = 2\pi/L_z$ corresponds to the spanwise wavenumber of the large-scale secondary flows, and the scale decomposition at this wavenumber gives a reasonable split of the large-scale secondary flows and localised turbulence.

The transport equations for $\overline{u_i^L u_j^L}$ and $\overline{u_i^S u_j^S}$ are derived by procedures similar to the derivation of the transport equation of the full Reynolds stress $\overline{u_i u_j}$, and are written as

$$\frac{D\overline{u_i^L u_j^L}}{Dt} = P_{ij}^L - \varepsilon_{ij}^L + \Pi_{ij}^L + D_{ij}^{p,L} + D_{ij}^{\nu,L} + D_{ij}^{t,L} - Tr_{ij}, \tag{3a}$$

$$\frac{D\overline{u_i^S u_j^S}}{Dt} = P_{ij}^S - \varepsilon_{ij}^S + \Pi_{ij}^S + D_{ij}^{p,S} + D_{ij}^{\nu,S} + D_{ij}^{t,S} + Tr_{ij}, \tag{3b}$$

where the first six terms in Eqs. (3a) and (3b) are the large- and small-scale parts of the corresponding terms in the standard Reynolds-stress transport equation; the large-scale parts in Eq. (3a) are defined as

$$P_{ij}^L = -\overline{u_i^L u_k^L}\frac{\partial U_j}{\partial x_k} - \overline{u_j^L u_k^L}\frac{\partial U_i}{\partial x_k}, \quad \varepsilon_{ij}^L = 2\nu \overline{\frac{\partial u_i^L}{\partial x_k}\frac{\partial u_j^L}{\partial x_k}},$$

$$\Pi_{ij}^L = \overline{\frac{p^L}{\rho}\left(\frac{\partial u_i^L}{\partial x_j} + \frac{\partial u_j^L}{\partial x_i}\right)}, \quad D_{ij}^{\nu,L} = \nu \frac{\partial^2 \overline{u_i^L u_j^L}}{\partial x_k^2}$$

$$D_{ij}^{p,L} = -\frac{1}{\rho}\frac{\partial}{\partial x_k}\left(\overline{u_i^L p^L}\delta_{jk} + \overline{u_j^L p^L}\delta_{ik}\right),$$

$$D_{ij}^{t,L} = -\frac{\partial}{\partial x_k}\left(\overline{u_i^L u_j^L u_k^L} + \overline{u_i^L u_j^L u_k^S} + \overline{u_i^S u_j^L u_k^S} + \overline{u_i^L u_j^S u_k^S}\right),$$

and the small-scale counterparts in Eq. (3b) are defined by interchanging the superscripts L and S in their large-scale counterparts defined above. In addition to them, the last term Tr_{ij} appears newly due to the large- and small-scale decomposition of the transport equation and is defined as

$$Tr_{ij} = -\overline{u_i^S u_k^S \frac{\partial u_j^L}{\partial x_k}} - \overline{u_j^S u_k^S \frac{\partial u_i^L}{\partial x_k}} + \overline{u_i^L u_k^L \frac{\partial u_j^S}{\partial x_k}} + \overline{u_j^L u_k^L \frac{\partial u_i^S}{\partial x_k}}. \tag{4}$$

As Tr_{ij} appears in the transport equations of $\overline{u_i^L u_j^L}$ and $\overline{u_i^S u_j^S}$ as $-Tr_{ij}$ and Tr_{ij}, respectively, it clearly represents the energy transfer from the larger- to smaller scales (more details are found in Kawata & Alfredsson, 2018, 2019). In the present analysis, we investigate the nonlinear scale interactions between the small-scale localised turbulence and the large-scale secondary flows through the large/small-scale decomposed Reynolds-stress transport equations Eqs. (3a) and (3b) particularly focusing on the roles of the interscale energy transfer terms Tr_{ij}.

RESULTS

The obtained flow field exhibits a typical turbulent stripe, as shown in Fig. 2(a). Here, to visualise both the large-scale secondary flows and the localised turbulence, we present the small-scale part of the fluctuating flow field by the

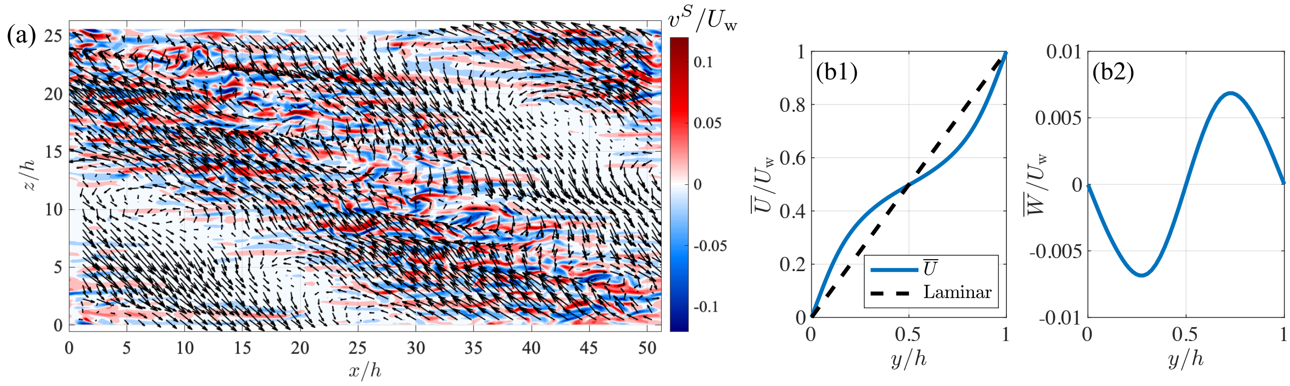

Figure 2. Instantaneous and mean flow field: (a) a snapshot of instantaneous velocity fluctuations on the channel centre plane $y/h = 0.5$, where the colours represent the small-scale part of wall-normal velocity fluctuation v^S and black arrows are drawn based on (u^L, w^L); (b1, b2) profiles of mean streamwise and spanwise velocities.

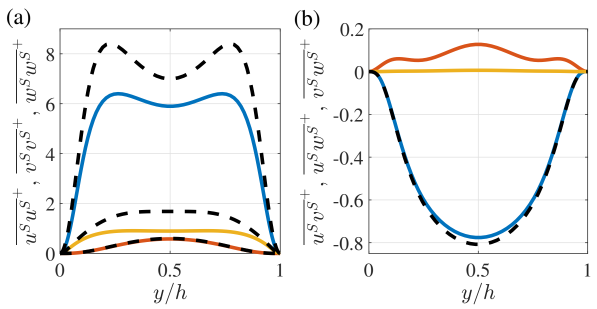

Figure 3. Profiles of small-scale parts of Reynolds stresses scaled by u_τ^2: (a) normal stress components (blue) $\overline{u^S u^S}$, (red) $\overline{v^S v^S}$ and (yellow) $\overline{w^S w^S}$; (b) shear stress components (blue) $\overline{u^S v^S}$, (red) $\overline{u^S w^S}$ and (yellow) $\overline{v^S w^S}$. The black dashed lines present the profiles of the major components of the full Reynolds stresses: $\overline{u^2}$, $\overline{v^2}$ and $\overline{w^2}$ in the panel (a) and $\overline{uv}$ in the panel (b).

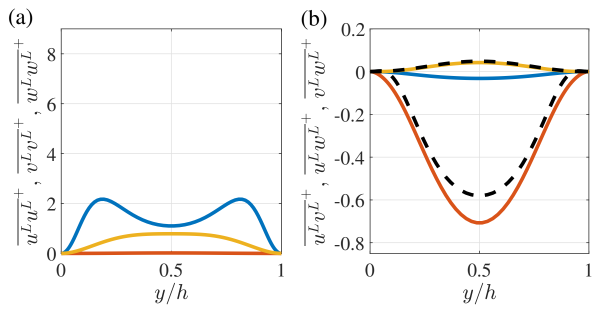

Figure 4. Profiles of small-scale parts of Reynolds stresses scaled by u_τ^2: (a) normal stress components $\overline{u^S u^S}$, $\overline{v^S v^S}$ and $\overline{w^S w^S}$; (b) shear stress components $\overline{u^S v^S}$, $\overline{u^S w^S}$ and $\overline{v^S w^S}$. The line colours indicate the same stress components as in Fig. 3. The black dashed line in the panel (b) present the profiles of the secondary shear stress components of the full Reynolds stress $\overline{uw}$ and $\overline{vw}$.

colours representing the instantaneous distribution of the wall-normal velocity fluctuation v^S, while the large-scale secondary flow structure is indicated by the black arrows representing (w^L, u^L). The distribution of v^S clearly presents a band-like turbulent region, and the existence of large-scale secondary flows along the laminar–turbulent interfaces are also indicated by (w^L, u^L). The panels (b1) and (b2) present the profiles of the mean streamwise velocity $\overline{U}$ and the mean spanwise velocity $\overline{W}$, respectively. The profile of $\overline{U}$ somewhat deviates from the laminar solution, and the profile of $\overline{W}$ indicates the presence of non-zero spanwise mean flows, while the magnitude is about 1% of the mean streamwise, despite the spanwise symmetry of the configuration.

Figure 3 presents the profiles of the small-scale parts of the Reynolds stresses $\overline{u_i^S u_j^S}$. As indicated by the profiles of $\overline{u^S u^S}$, $\overline{v^S v^S}$ and $\overline{w^S w^S}$ in the panel (a), the small-scale part of the velocity fluctuation accounts for most of the turbulent kinetic energy. Nearly 80% of the streamwise turbulent energy $\overline{u^2}$ is accounted for by its small-scale part $\overline{u^S u^S}$, and the wall-normal turbulent energy $\overline{v^2}$ is almost fully dominated by $\overline{v^S v^S}$. As indicated by the $\overline{w^S w^S}$, about half of the spanwise turbulent energy $\overline{w^2}$ is also attributed to the small-scale turbulent motions. Summarising the tendencies indicated by the profiles of $\overline{u^S u^S}$, $\overline{v^S v^S}$ and $\overline{w^S w^S}$ in terms of their shapes and relative magnitudes, the overall trend is qualitatively similar to the typical turbulent energy distribution observed in fully-developed wall-bounded turbulence.

Turning to the shear stresses components presented in Fig. 3(b), $\overline{u^S v^S}$ is shown to be the most prominent among the three shear stress components by having a significantly larger magnitude. The secondary shear stress component $\overline{v^S w^S}$ is nearly zero throughout the channel, and the other secondary shear stress $\overline{u^S w^S}$ is also fairly small in magnitude throughout the channel—although $\overline{u^S w^S}$ is not exactly zero unlike $\overline{v^S w^S}$. Except the non-zero $\overline{u^S w^S}$ component, these profiles of the Reynolds shear stresses exhibit fairely similar trends as those typically found in canonical wall turbulence. It is also shown that the primary Reynolds shear stress $\overline{uv}$ is almost entirely accounted for by the small-scale part $\overline{u^S v^S}$, indicating that the transport of the streamwise momentum in the flow is thoroughly due to the small-scale fluid motions.

On the other hand, the large-scale parts of the Reynolds stresses presented in Fig. 4 exhibit entirely different characteristics. Unlike their small-scale counterparts, $\overline{u^L u^L}$ and $\overline{w^L w^L}$ are of comparable magnitude, while $\overline{v^L v^L}$ is nearly zero throughout the channel. This indicates that the large-scale structure has velocity fluctuations of similar intensities in the streamwise and spanwise directions, whereas its wall-normal fluid motions are extremely weak. Furthermore, as indicated by the profiles of the shear components in the right panel, $\overline{u^L v^L}$

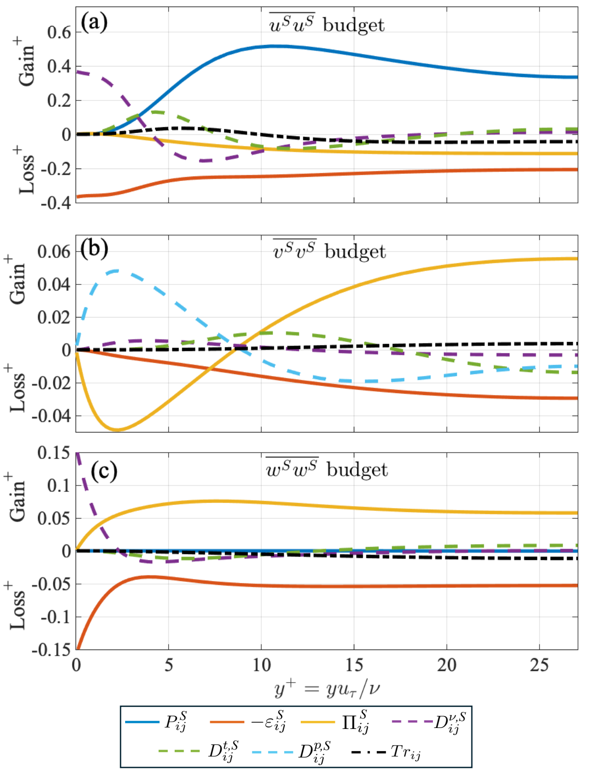

Figure 5. Budget balances of transport equations for small-scale turbulent energies scaled by u_τ^4/ν: (a) $\overline{u^S u^S}$, (b) $\overline{v^S v^S}$ and (c) $\overline{w^S w^S}$. Only the lower half of the channel $0 \le y/h \le 0.5$ is shown in the wall units.

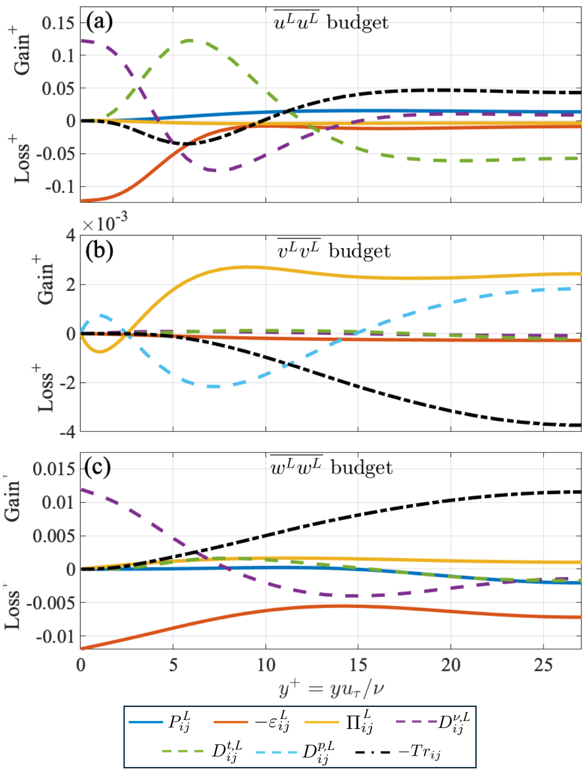

Figure 6. Budget balances of transport equations for large-scale turbulent energies scaled by u_τ^4/ν presented in the same manner as in Fig. 5: (a) $\overline{u^L u^L}$, (b) $\overline{v^L v^L}$ and (c) $\overline{w^L w^L}$.

is nearly zero, unlike the canonical wall turbulence, and most importantly the secondary shear stress components $\overline{u^L w^L}$ and $\overline{v^L w^L}$ exhibit significant magnitudes—in particular, the magnitude of $\overline{u^L w^L}$ is comparable to the primary shear stress $\overline{uv}$ (compare Figs. 3(b) and 4(b)). These nonzero secondary shear stresses clearly indicate a symmetry breaking in the spanwise direction. Particularly, the negative $\overline{u^L w^L}$ corresponds to the secondary flows along the turbulent band presented in Fig. 2(a)—$u^L > 0$ and $w^L < 0$ on the upstream side and $u^L < 0$ and $w^L > 0$ on the downstream side both result in $\overline{u^L w^L} < 0$.

Now, we investigate the budget balance of the turbulent energy transport for each large- and small-scale side based on Eqs (3a) and (3b). Figure 5 presents the budget balances of the transport equations of the small-scale parts of these turbulent energies $\overline{u^S u^S}$, $\overline{v^S v^S}$ and $\overline{w^S w^S}$. These budget balances exhibit qualitatively similar tendencies to those typically observed in the canonical wall turbulence (see, for example, Pope, 2000); only the streamwise turbulent energy $\overline{u^S u^S}$ has the energy gain by the mean velocity gradient, $P_{uu}^S = -2\overline{u^S v^S}\mathrm{d}\overline{U}/\mathrm{d}y$, and the energy injected into $\overline{u^S u^S}$ via P_{uu}^S is partly redistributed to $\overline{v^S v^S}$ and $\overline{w^S w^S}$ via the pressure-strain correlations Π_{vv}^S and Π_{ww}^S, which are eventually transported in physical space by diffusion terms and finally dissipated by the viscous dissipations. The interscale flux terms in these transport equations, Tr_{uu}, Tr_{vv} and Tr_{ww}, are shown to be negligibly small compared to the other terms and to have only very minor contributions to the budget balances. The observations described here suggest that the sustaining mechanisms of the localised small-scale turbulence are fundamentally similar to those of the canonical wall turbulence.

The budget balances for the large-scale counterparts, $\overline{u^L u^L}$, $\overline{v^L v^L}$ and $\overline{w^L w^L}$, presented in Fig. 6 exhibit, on the other hand, qualitatively different tendencies from the typical budget balances of wall turbulence. In the budget balance for $\overline{u^L u^L}$ in Fig. 6(a), the diffusion terms $D_{uu}^{\nu,L}$ and $D_{uu}^{t,L}$ exhibit remarkable contributions in comparison to the other terms, unlike in the budget on the small-scale side, but their qualitative tendencies are similar to their small-scale counterparts—the turbulent diffusion $D_{uu}^{t,L}$ transfers energy from the central to the near-wall regions of the channel and the viscous diffusion $D_{uu}^{\nu,L}$ further transports energy towards the wall vicinity, where the energy is dissipated by the viscous dissipation ε_{uu}^L. The essential difference from the typical budget balances is indicated by the main energy source. As shown by the blue solid line in Fig. 6(a), the production term P_{uu}^L—the primary energy source in the typical energy budget balance—shows clearly smaller magnitudes than the diffusion and dissipation terms. The role of the main energy gain is, instead, played by the interscale energy flux term, $-Tr_{uu}$, which clearly exhibits an energy gain that exceeds the contribution of P_{uu}^L in magnitude in the central region of the channel. This indicates that more energy is transferred from small-scale turbulence to the large-scale flows than from the mean flow. Although $-Tr_{uu}$ exhibits a negative contribution, i.e., an energy transfer from $\overline{u^L u^L}$ to $\overline{u^S u^S}$, in the near-wall region, the integral of $-Tr_{uu}$ over the channel gives a positive contribution, indicating that the net energy transfer over the entire range of the channel is from $\overline{u^S u^S}$ to $\overline{u^L u^L}$, consistently with previous investigation on the energy transport by Gomé *et al.* (2023).

The interscale energy flux also plays a striking role in the transport of the large-scale spanwise velocity fluctuation $\overline{w^L w^L}$. As shown in Fig. 6(c), the interscale energy flux term exhibits energy transfers from the small-scale side to the large-scale side over the entire range of the channel, clearly playing the role as the primary energy source for the large-scale span-

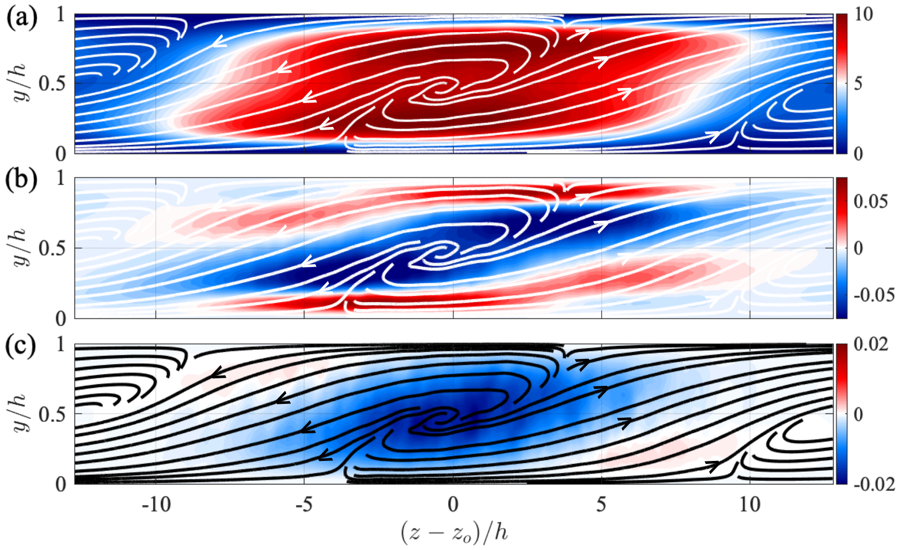

Figure 7. Cross-sectional distributions of velocity fluctuation and interscale energy fluxes: (a) small-scale part of turbulent energy $\langle u^S u^S \rangle$; (b) interscale flux of streamwise turbulent energy $Tr_{uu,\mathrm{st}}$; (c) interscale flux of spanwise turbulent energy $Tr_{ww,\mathrm{st}}$. Here, z_o is the spanwise coordinate of the centre of the turbulent band region, and the value are scaled based on u_τ and ν. The white or black lines in each panel present streamlines drawn based on $(\langle w^L \rangle, \langle v^L \rangle)$.

wise fluid motions. By comparing Figs. 6(a) and (c), one can see that the magnitude of Tr_{ww} is comparable to that of Tr_{uu}. Such energy gains for $\overline{u^L u^L}$ and $\overline{w^L w^L}$ with comparable magnitudes are attributable to the fact that $\overline{u^L u^L}$ and $\overline{w^S w^S}$ are of comparable magnitudes as investigated in Fig. 4(a).

In contrast to Tr_{uu} and Tr_{ww}, the interscale energy flux for the wall-normal fluid motion exhibits energy transfer from the large-scale side to the small-scale side, as shown in Fig, 6(b). The primary energy source for $\overline{v^L v^L}$ is the energy redistribution from $\overline{u^L u^L}$ via Π^L_{vv}, similarly to the budget balance on the small-scale side. The energy gain through Π_{vv}, i.e., the energy redistribution from $\overline{u^L u^L}$ or $\overline{w^L w^L}$, presumably represents the effect of pressure redirecting fluid motions in the x- or z-directions into the y-direction to satisfy the continuity. The energy gain by Π^L_{vv} is balanced by $-Tr_{vv}$, indicating that the large-scale wall-normal fluid motions breaks into small-scale wall-normal fluid motions by the turbulent energy cascade.

It is worth recalling here that the contributions of these interscale energy flux terms, Tr_{uu}, Tr_{vv} and Tr_{ww}, are fairly negligible in the budget balance on the small-scale side, as investigated in Fig. 5(a). In fact, the net energy amount transferred from the small- to large-scale velocity fluctuations via Tr_{uu} and Tr_{ww} is only about 7% of the total amount of the energy injected from the mean flow to the velocity fluctuations. Hence, the energy transfers between the mean flows and the large/small-scale part of the velocity fluctuations investigated above suggest that the uniform shear by the flat plates generates the small-scale turbulence first, and the large-scale secondary flows then emerge from the small-scale turbulence by receiving a slight amount through nonlinear scale interactions.

It is also noteworthy in the $\overline{w^L w^L}$ transport budget presented in Fig. 6(c) that the energy production P^L_{ww} exhibits negative values in the channel core region, which indicates that kinetic energy is transferred from the spanwise fluid motions of the large-scale secondary flows to the spanwise mean flow $\overline{W}$. The small-scale counterpart P^S_{ww} (the energy transfer between $\overline{w^S w^S}$ and the spanwise mean flow $\overline{W}$) is, on the other hand, not significant compared to P^L_{ww}. This is because these productions are written as

$$P^L_{ww} = -2\overline{v^L w^L}\frac{\mathrm{d}\overline{W}}{\mathrm{d}y}, \qquad P^S_{ww} = -2\overline{v^S w^S}\frac{\mathrm{d}\overline{W}}{\mathrm{d}y}, \tag{5}$$

and $\overline{v^S w^S}$ is far smaller than $\overline{v^L w^L}$, as can be seen by comparing Figs. 3(b) and 4(b). In fact, this negative energy production P^L_{ww} is the primary energy source in the transport budget of the spanwise mean flow energy $\overline{W}^2$ (not shown). Hence, the kinetic energy associated with the spanwise fluid motions is consistently transferred from smaller to larger scales: from the localised turbulence to the large-scale secondary flows, and further from the large-scale secondary flows to the spanwise mean flows.

Finally, we adopt a spatial averaging along the turbulent band region as considered in many earlier studies (e.g., Barkley & Tuckerman, 2007; Gomé *et al.*, 2023), to visualise the averaged flow patterns of the large-scale secondary structures. In the following, we retain the direction of the x- and z-axes unlike in the previous studies where these directions denote those along and perpendicular to the turbulent band, but we average statistics in space along the band as well as in time to investigate the spatial structures of the large-scale structures and turbulent band. We denote the quantities averaged in space along the turbulent band and in time as $\langle \cdot \rangle$ in the following; it should be noted here that averaging $\langle \phi \rangle$ further in the z-direction $\langle \phi \rangle$ results in $\overline{\phi}$.

Figure 7 presents the cross-sectional distributions of the along-band-averaged velocity fluctuation $\langle u^S u^S \rangle$ and interscale energy fluxes $Tr_{uu,\mathrm{st}}$ and $Tr_{ww,\mathrm{st}}$, which are defined by replacing the averaging operators $\overline{\cdots}$ by $\langle \cdots \rangle$ in Eq. (4). The white or black lines with arrows in each panel indicate streamlines drawn based on the distributions of $\langle v^L \rangle$ and $\langle w^L \rangle$, which reveal the averaged cross-sectional flow pattern of the large-scale secondary flows. As shown by Figs. 7(a), the streamlines emerge from the centre of the turbulent region and are directed towards the upper right and the lower left of the figure. This cross-sectional flow pattern clearly leads to a positive correlation between v^L and w^L, which is consistent with the profile of

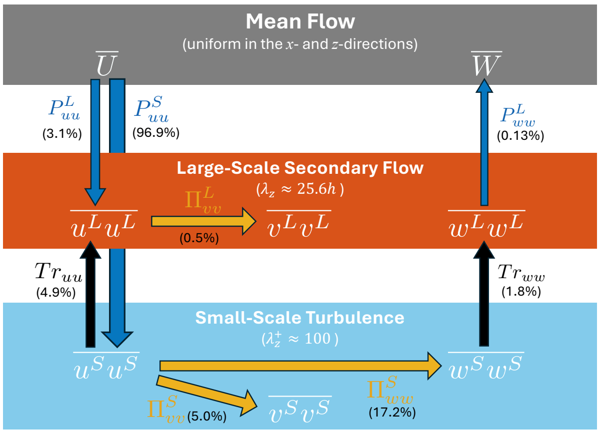

Figure 8. Energy flow map in the transitional turbulent plane Couette flow. The arrows with different colours represent flow of energy transfer by different terms in Eqs. (3a) and (3b). The numbers in parentheses indicate relative amount of energy transfer (integrated across the channel) to the total primary turbulent energy production $P_{uu} = P^L_{uu} + P^S_{uu}$.

$\overline{v^L w^L}$ presented in Fig. 4(b). In fact, $\overline{v^L w^L} \approx \langle v^L \rangle \langle w^L \rangle$, indicating that the cross-streamwise secondary flow indicated by the streamlines are primarily responsible for the non-zero secondary Reynolds stress component $\overline{vw}$.

As shown in Figs. 7(b) and (c), both $Tr_{uu,\mathrm{st}}$ and $Tr_{ww,\mathrm{st}}$ indicate negative energy flux, i.e., energy transfer from smaller to larger scales, within the localised turbulent region. In particular, the energy flux of the streamwise turbulent energy $Tr_{uu,\mathrm{st}}$ exhibits forward transfer from the large to small scales in the near-wall region, whereas the spanwise energy transfer $Tr_{ww,\mathrm{st}}$ shows inverse energy transfer throughout the turbulent region. One can see from these figures that the inverse interscale energy transfers from the small- to large-scale side take place in the core of the localised turbulent region.

DISCUSSION AND CONCLUSION

The energy transfers observed by the present analysis may be summarised as illustrated in Fig. 8. The streamwise mean flow—which is uniform in both the streamwise and spanwise directions—gives kinetic energy to the large-scale secondary flows and the small-scale localised turbulence through the turbulent energy production $P_{uu} = -2\overline{uv}\mathrm{d}\overline{U}/\mathrm{d}y = P^L_{uu} + P^S_{uu}$, and about 97 % of the energy amount produced by the total production P_{uu} goes directly to the small-scale turbulence via P^S_{uu}. The kinetic energy injected to the small-scale turbulence is redistributed among different velocity components and eventually dissipated by viscosity, similarly in canonical wall turbulence. The amount of kinetic energy supplied to the large-scale flows is, on the other hand, only about 10 % of the total energy production; 3 % is the energy transfer from the mean flow via P^L_{uu} and the rest 7 % is the inverse interscale energy transfers from the small-scale side via Tr_{uu} and Tr_{ww}. About 10 % of the energy transferred from $\overline{w^S w^S}$ to $\overline{w^L w^L}$ via Tr_{ww} is further transferred to the spanwise mean flow by the negative energy production P^L_{ww}. As a whole, 0.13 % of energy extracted from the mean flow to the velocity fluctuations comes back to the mean flow as spanwise mean fluid motions.

The above-described energy transfer suggests that the uniform shear by the walls first generates small-scale turbulence, and the oblique and large-scale secondary flows are produced by the small-scale turbulence. This is certainly in line with the investigation by Parente *et al.* (2022) that spatially localised perturbations give rise to the large-scale flows and seemingly conflicts those studies suggesting that the oblique large-scale flows generate and sustain the band-like localised turbulence such as Duguet & Schlatter (2013) and Xiao & Song (2020), for instance. However, these studies investigated temporal growths of turbulent spots or turbulent bands of finite lengths, whereas in the present study a periodic turbulent band at a statistically steady state is investigated. Nevertheless, in the present study the role of inverse interscale energy transfers from the small-scale localised turbulence to the large-scale secondary flows has been revealed. At least in the turbulent band structures at statistical steady state as in the present simulation, the large-scale secondary flows along the oblique turbulent band are sustained by receiving kinetic energy from localised small-scale turbulence, rather than produces it.

REFERENCES

Barkley, D. & Tuckerman, L. S. 2007 Mean flow of turbulent–laminar patterns in plane Couette flow. *J. Fluid Mech.* **576**, pp. 109–137.

Couliou, M. & Monchaux, R. 2015 Large-scale flows in transitional plane Couette flow: A key ingredient of the spot growth mechanism. *Phys. Fluids* **27**, 034101.

Duguet, Y. & Schlatter, P. 2013 Oblique laminar-turbulent interfaces in plane shear flows. *Phys. Rev. Lett.* **110**, 034502.

Fukudome, K., Iida, O. & Nagano, Y. 2009 The mechanism of energy transfer in turbulent Poiseuille flow at very low-Reynolds number. *In Proc: The 6th International Symposium on Turbulence and Shear Flow Phenomena* pp. 471–476.

Gomé, S., Tuckerman, L. S. & Barkley, D. 2023 Patterns in transitional shear turbulence. part 1. energy transfer and mean-flow interaction. *J. Fluid Mech.* **964**, A16.

Kawata, T. & Alfredsson, P. H. 2018 Inverse interscale transport of the Reynolds shear stress in plane Couette turbulence. *Phys. Rev. Lett.* **120**, 244501.

Kawata, T. & Alfredsson, P. H. 2019 Scale interactions in turbulent rotating planar Couette flow: insight through the Reynolds stress transport. *J. Fluid Mech.* **879**, pp. 255–295.

Klotz, L., Pavlenko, A.M. & Westreid, J.E. 2021 Experimental measurements in plane Couette–Poiseuille flow: dynamics of the large- and small-scale flow. *J. Fluid Mech.* **912**, A24.

Nimura, T., Kawata, T. & Tsukahara, T. 2019 Interscale energy transport for turbulent stripe in rotating plane Couette flow. *In Proc: The 17th European Turbulence Conference* .

Parente, E., Robinet, J.-Ch., Palma, P. De & Cherubini, S. 2022 Linear and nonlinear optimal growth mechanisms for generating turbulent bands. *J. Fluid Mech.* **938**, A25.

Pope, S. B. 2000 *Turbulent Flows*. Cambridge University Press.

Tsukahara, T., Sek, Y., Kawamura, H. & Tochio, D. 2005 DNS of turbulent channel flow at very low Reynolds numbers. *In Proc: The 4th International Symposium on Turbulence and Shear Flow Phenomena* .

Tuckerman, L. S., Chantry, M. & Barkley, D. 2020 Patterns in wall-bounded shear flows. *Annu. Rev. Fluid Mech.* **52**, pp. 343–367.

Xiao, X. & Song, B. 2020 The growth mechanism of turbulent bands in channel flow at low Reynolds numbers. *J. Fluid Mech.* **883**, R1.